LA-UR-22-21532

Approved for public release; distribution is unlimited.

Title:	Pit depth analysis using automated software for three containers with complete imaging
Author(s):	Kaufeld, Kimberly Ann Kelly, Elizabeth J. Wendelberger, James G.
Intended for:	Report
Issued:	2022-02-23

Pit depth analysis using automated software for three containers with complete imaging

Kimberly A. Kaufeld, Elizabeth J. Kelly, James G. Wendelberger

Abstract

The 3013 surveillance program is tasked with ensuring the long term safety of plutonium storage in 3013-compliant containers. One component of this task is to understand corrosion features found on the interior sidewall of the inner container closure weld region (ICCWR). To this end, three containers were selected to have laser confocal microscope (LCM) 20X imaging of the entire ICCWR. This report describes the analysis of the LCM pit depth data using the automated corrosion analysis software. The analysis included determining maximum pit depths and distributions of pit depths, volumes, and diameters for all pit features identified on the three containers. Results provided insight into possible corrosion mechanisms and were consistent with previous pit growth model predictions.

1: Introduction

The 3013 standard requires the development of a surveillance program to validate technical assumptions and assure the long-term safety of plutonium storage in 3013-compliant containers. In response to this requirement, an Integrated Surveillance Program (ISP) has been developed. The most recent guidance for the ISP is the "Integrated Surveillance and Monitoring Program for Materials Packaged to Meet DOE-STD-3013" (DOE, 2015). This document (also referred to as the ISP) draws extensively from the "Test Plan for Assessing Potential for Stress Corrosion Cracking in the 3013 Inner Container Closure Weld Region (FY 2014)" (Berg, et. al 2014). As described in both the ISP and test plan the bounding region for identifying stress corrosion cracking (SCC) and pitting has been determined to be the inner container closure weld region (ICCWR). Figure 1 shows the ICCWR and identifies some of the conditions in the ICCWR that the Corrosion Working Group (CWG) Subject Matter Experts (SMEs) consider bounding.

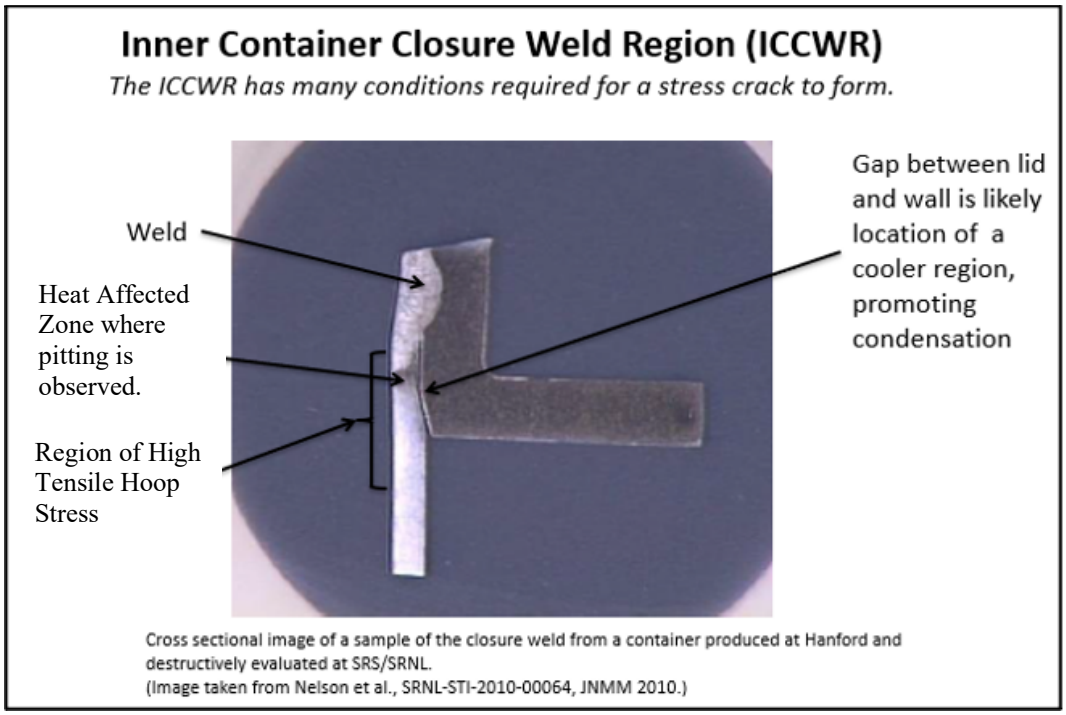

Figure 1: The inner container closure weld region (ICCWR).

One task identified in the test plan (Berg, et. al 2014) is to understand corrosion features found on the interior sidewall of the ICCWR (we will refer to the interior sidewall of the ICCWR simply as the ICCWR), including how they are distributed. For this task, three containers were selected to have laser confocal microscope (LCM) 20X imaging of the entire ICCWR. The CWG SME's selected the three containers based on the conditions observed in each container at the time of Destructive Examination (DE). These conditions were considered to be worst-case in terms of possible corrosion impacts. This report describes the analysis of the LCM pit depth data for the entire ICCWR using the automated corrosion analysis software (Wendelberger 2020).

2: LCM Imaging

Savannah River National Laboratory conducts LCM imaging of the ICCWR during destructive examination of the containers using the Keyence 3D laser confocal microscope model VKX110 (Martínez-Rodríguez, M.J, 2017, 2018 and 2019). In order to perform the LCM imaging, the lid is cut into 4 sections and each section is cut into 2 subsections labeled A1 to D2 as in Figure 2.

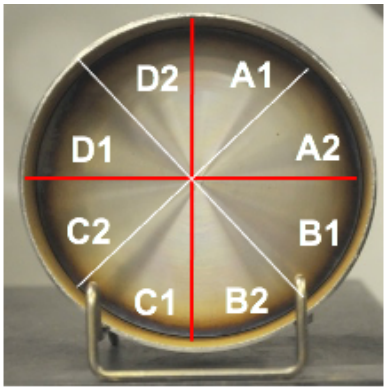

Figure 2: Cuts for the ICCWR sections A1-D2.

The ICCWR is divided into three zones (Figure 3). Zone 1 is the section of the container that has been fabricated to have a slightly larger inner diameter with thinner container walls to allow for the closure plug to be inserted. Zone 2 is the transition area between the thinner container wall and the thicker lower wall, approximately 1500 microns (1.5mm) in length. This area is flow formed and then machined resulting in a beveled area. This area is responsible for stopping the inserted plug from going too far

into the container. Zone 3 is the native container surface below the machined area. In most of the containers examined to date, the weld goes into Zone 2, so that Zone 1 is missing as is part of Zone 2.

The ICCWR region is considered the most likely location for inner container failure from stress corrosion cracking (SCC) because welding can increase local residual stress fields and creates a heat-affected zone that may have increased corrosion susceptibility (Berg et al. 2014).

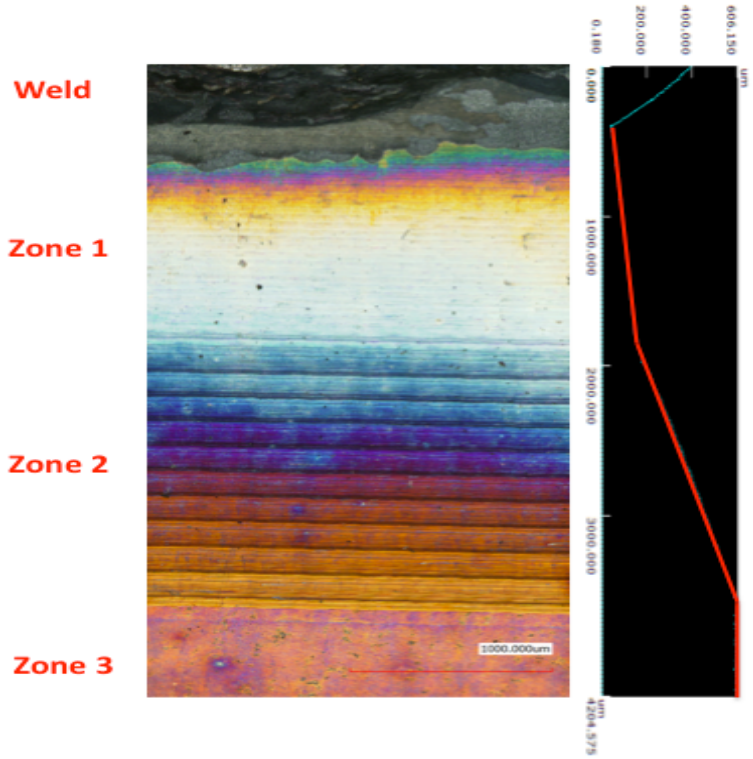

Figure 3: Representative optical image of the ICCWR region with Zones 1-3 delineated. The image on the left shows the weld and the zones away from the weld. On the right is a profile plot that shows the thickness of the container wall. The thickness is larger and is constant for Zone 3, decreases across Zone 2, and is thinnest and leveling off in Zone 1. Note that this figure is unusual since the weld is generally in Zone 1 and often partially into Zone 2. Picture from (Duque et al, 2018).

Because of curvature issues while utilizing the LCM, the image data is collected across 14 sub-subsections for Zone 3 and four sub-subsections for Zone 1 & 2 (Figure 4). Zone 3 images include the interface between Zone 3 and Zone 2. DE and corrosion studies have indicated that the top six millimeters (6000 microns) of Zone 3 and the Zone 2/Zone 3 interface are the worst-case areas for corrosion. The Zone 3 LCM images provide better imaging for the automated corrosion analysis software and include the Zone 2 interface. Therefore, the pit depth analysis in this report is for the Zone 3 images, which include the first six millimeters of Zone 3.

In Zone 3 images there are generally 112 image sections per container. There are 8 cut subsections and each subsection requires 14 images (which will be called sub-subsections) to be taken due to curvature, resulting in the 112 imaged regions. In this report all the image sections in Zone 3 are assessed for pitting, however, the edges, sub-subsections 1 and 14, are looked at individually as part of these sub-subsections are off the physical sample in these images. For example, in Figure 4, the black area on sub-subsections 1 and 14 are off sample.

Figure 4: Zone 3 (top) divided into 14 sections for LCM imaging and Zone 1&2 (bottom) is divided into 4 sections for LCM imaging.

In each of the 112 image sections there are many 20X LCM images. For example, in subsection D2, sub-subsection 12 there are 45 20X LCM images (Figure 5). For an entire ICCWR there are over 9,000 20X LCM images. This makes the human analysis of LCM 20X data for a complete ICCWR for a large number of containers logistically infeasible. Therefore, software has been developed to automate the process (Wendelberger 2020). This report presents the pit depth results for the three complete ICCWRs based on the automated corrosion analysis software results.

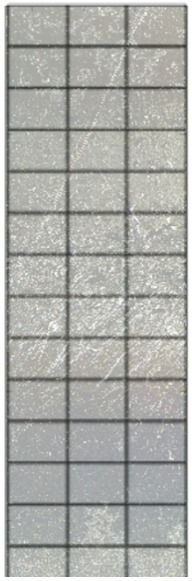

Figure 5: Montage image that is composed of several smaller 20x images from D2 sub-subsection 12.

Montage or stitched images are created from a collection of individual 20x images. These montage images exist for each sub-subsection. For example, on container FY15DE08, subsection D2 sub-subsection 12 there are 45 20X images stitched together to make the montage (see Figure 5). The individual 20x LCM images have pixels that are 0.7 microns on each side (an area of 0.49 sq microns), whereas the montage (stitched) image results in pixels that are between 2 and 5 microns per side (areas between 4 and 25 sq microns). Therefore, a montage pixel contains between approximately 8 and 50 individual 20X pixels.

In terms of pit depth assessment, there is an efficiency in analyzing the montage as compared to analyzing the 20x LCM images. There are 112 images per container for the montage versus greater than 9000 images for the 20x LCM images. Pit features on the montages are easier to evaluate. For example, working with 112 files versus 9000 makes it easier to organize the files and understand the output. It also reduces analysis time for the analyst as there are many fewer image result files to look at.

The Keyence microscope has software that an analyst can use to determine pit depths. These analyses require considerable analyst time. The Keyence software was used to evaluate pit depths for a small subset of the LCM 20X images. Another pit depth analysis tool is Gwyddion (http://Gwyddion.net). Pit depths for some of the LCM 20X images were also analyzed using Gwyddion. The automated software was compared to the Keyence and Gwyddion results for the montage and 20X LCM images. The measurements generally agreed when the pit features had depths greater than 20 to 30 microns (Kaufeld et al 2021a, Kaufeld et al 2021b, Kaufeld et al 2021c). Features of this size can have small differences, within 5-10 microns, that occur due to the differences in smoothing (curvature estimation methodology) and resolution. This report

describes the pit depth analysis using the montage data and focuses on pits with depths greater than 20 microns.

3: Automated Pit analysis software

The automated corrosion analysis software finds pit features on individual 20x images and montage (stitched) images based on height data (Wendelberger et al 2020). To do this it first reads in a vk4 formatted binary file that comes from the Keyence microscope, and converts it to height, optical, laser optical and intensity data. The height data is used to identify pit features and determine the depth of the features, which only the height data provides.

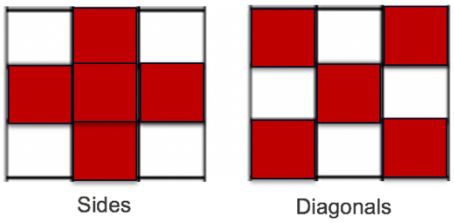

Figure 6: Examples of the way pixels can be connected to create a neighborhood.

The automated software first removes the curvature from the height data by smoothing so that the curvature from the sub-subsection image is removed. This is needed to get accurate depth values. Next, it connects pixels (i.e. makes pit features) with depths that are greater than a user specified value (e.g., 10 microns was used in this analysis). These pit features (aka features) are neighborhoods of pixels that either have sides that touch or touch at corners as shown in Figure 6. The user can set thresholds for features. For example, in the montage analysis, features where the max depth for at least one pixel in the feature is greater than or equal to 20 microns and the number of pixels in the feature is greater than or equal to 5 were included in the analysis. Once the thresholds have been set, the user can flag features of interest using depth (e.g. features that have maximum depth greater than 50 microns will show up red) so the features are easy to see. As a final output, the information about the features of interest based upon the specified parameters are written to an EXCEL file so they can be postprocessed for analysis.

4: Analysis of ICCWR containers

4.1 Overview of features

Three containers FY15DE07 (H003737), FY16DE05 (H003775), and FY15DE08 (H003896) have ICCWRs that were fully imaged using LCM 20X images. Montages for sub-subsections for these containers were also generated. The automated image analysis software was used to look at both the montage and individual 20X images for comparison. In general, pit features from the montage results were comparable to those from the 20X results (Kaufeld et al 2021a, Kaufeld et al 2021b). Stitching reduces resolution; however, it smooths the images, which can smooth out noise in the depth information.

4.2 Findings

An overview of the pit features of each of the container ICCWRs was conducted to assess where the deepest features are located. The automated software provides (among other statistics) depths, volumes, and equivalent diameters for each feature. The depths of the features are determined by taking the maximum depth across all the feature pixels, the volume is found by adding up the volumes of all the pixels. The equivalent diameter is calculated as $\sqrt{4 \times AREA/\pi}$

where area is calculated as the number of pixels times the area per pixel. Table 1 provides this information for the deepest features for each container.

Table 1. Statistics for the deepest pit depth measured from the montage images in each of the three complete ICCWR containers. The asterisk (*) indicates that the deepest pit for FY15 DE07 also has the largest volume.

Container	Deepest pit depth (microns)	Volume	Equivalent Diameter (microns)
FY15 DE07	57	0.00054*	155
FY16 DE05	63	0.000005	14
FY15 DE08	82	0.000022	34

Table 2. Statistics for the largest volume measured from the montage images in each of the three complete ICCWR containers. The asterisk (*) indicates that this pit also has the greatest depth or largest equivalent diameters for the container.

Container	Volume (cubic millimeters)	Pit depth (microns)	Equivalent Diameter (microns)
FY15 DE07	0.00054	57*	155
FY16 DE05	0.00015	20	120*
FY15 DE08	0.00032	22	160*

Table 3. Statistics for the largest equivalent diameters measured from the montage images in each of the three complete ICCWR containers. The asterisk (*) indicates that this pit also has the largest volume for the container.

Container	Equivalent Diameter (microns)	Pit depth (microns)	Volume (cubic millimeters)
FY15 DE07	164	34	0.00039
FY16 DE05	120	20	0.00015*
FY15 DE08	160	22	0.00032*

The deepest pit was found on FY15 DE08 D2 section 12 at 82 microns. It is a crescent shaped feature that was composed of 112 pixels and has an equivalent diameter of 34 microns. Figure 7a shows the software-generated pixel outline of this deepest feature from the montage analysis (red feature on left) and the height image from the montage on the right. The axis are associated with the pixel number. For example, FY15 DE08 D2 section 12 for the montage has 704 rows (x-coordinate) and 2432 columns (y-coordinate) where each row and column is a pixel.

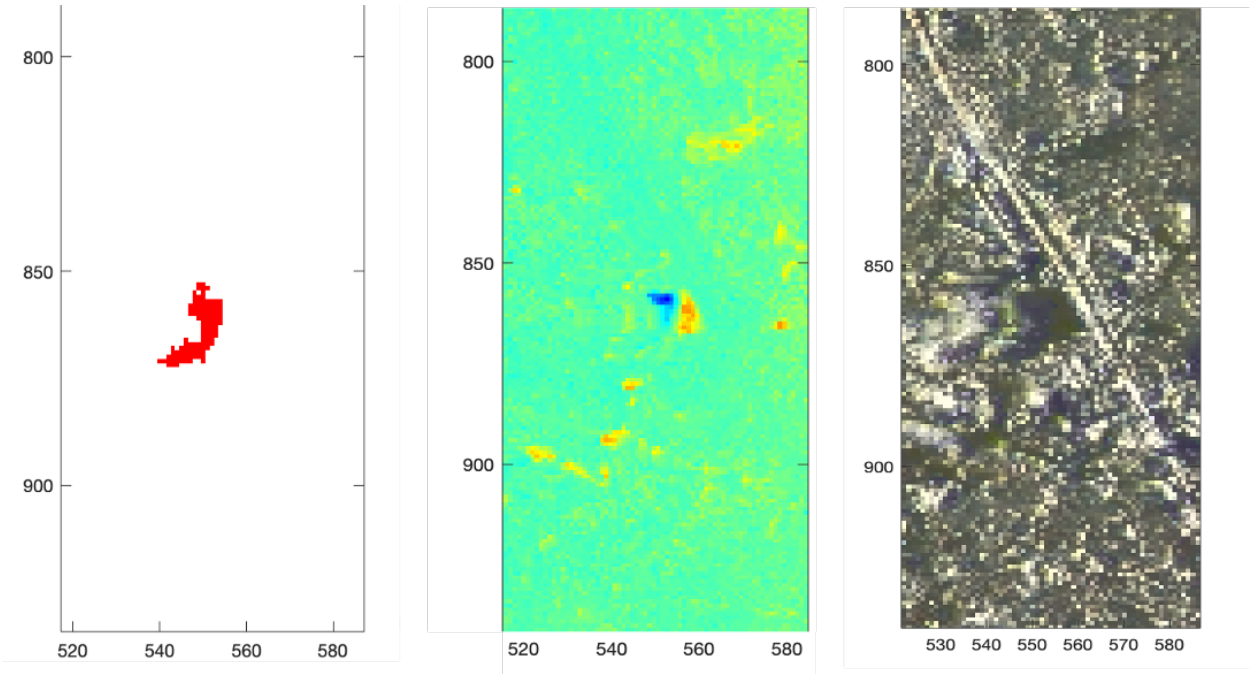

Figure 7a: Software generated pixel level feature from FY15 DE08 Section 12 with a depth of 82 microns from the Montage image (left) height image for the Montage image (middle), and optical image (right). The blue features are features below the surface, the yellow and orange features are above surface features.

The depth was confirmed with the individual 20X LCM image, which found the deepest pixel depth to be 89 microns (Figure 7 b). In Figure 7b on the left in red is the individual pixel outline from the individual 20X image and on the right is the individual 20X image height image. The individual 20X LCM height image shows the feature of interest, indicated in blue, is located next to a high feature, indicated in orange and red, which could be an indicator of debris (Figure 7 b). The minor difference between the depth of the montage image (Figure 7a) and the 20X LCM individual image (Figure 7b) is likely a result of the different pixel sizes.

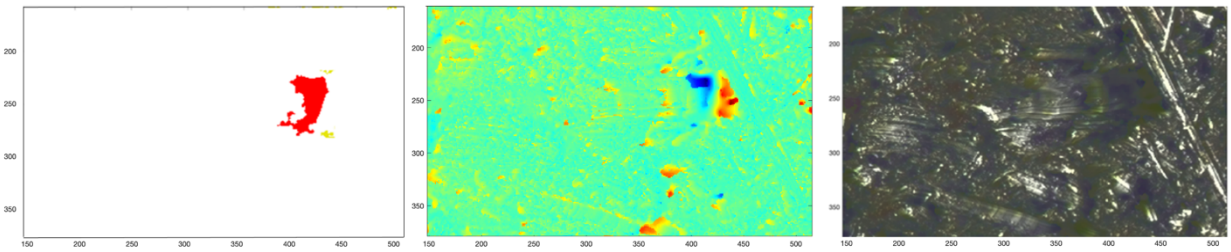

Figure 7b: Software generated pixel level feature from FY15 DE08 at a depth of 89 microns from the individual 20X LCM image (left), height image for the individual 20X LCM image (middle) and optical image (right). The blue features are features below the surface, the yellow and orange and red features are above surface features.

The deepest pit for FY15 DE07 was found in B1 subsubsection 8 at 57 microns for the montage and 59 microns on the individual 20X LCM. It is a circular shaped feature that was composed of 617 pixels for the montage. The montage software generated pixel image is shown on the left, height image in the middle and the and laser optical image for the feature is on the right in Figure 8a. The feature is a large deep feature, the area with the greatest depth is shown in dark blue in the height image. The laser optical image shows a large dark area, also indicating a pit.

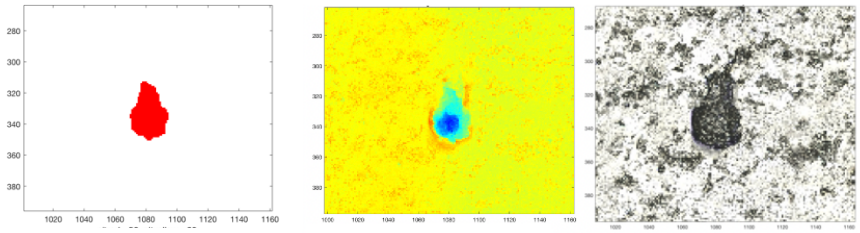

Figure 8a: Features from FY15DE07 Montage image with a depth of 57 microns. The montage pixel feature identification (left), height data (middle) and optical image (right).

Figure 8b shows the images for the individual 20X LCM image, with the software generated pixel image on the left, the height image in the middle, where below the surface features are blue and above the surface features are red, and the optical image on the right.

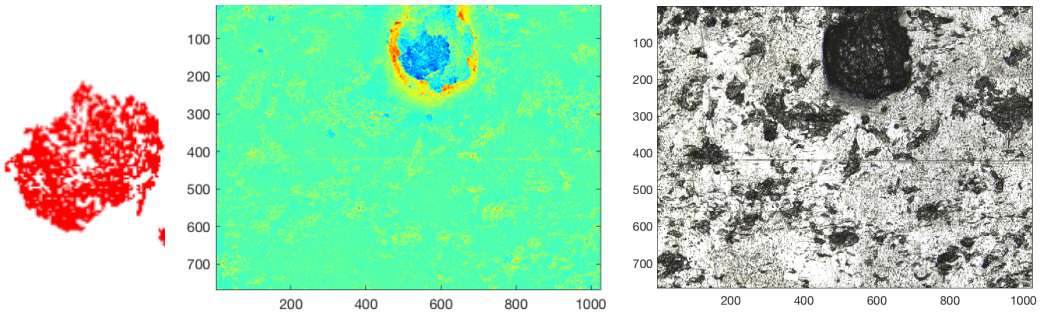

Figure 8b: Features from FY15DE07 individual 20X image with a depth of 59 microns. The individual 20X pixel feature identification zoomed in (left), height data where blue features are deep and red are high (middle) and optical image (right).

The deepest feature for FY16 DE05 was found in B2 subsubsection 13 at 63 microns for the montage and 65 microns for the individual 20X LCM. This feature was small, only 21 montage pixels in size (Figure 9a).

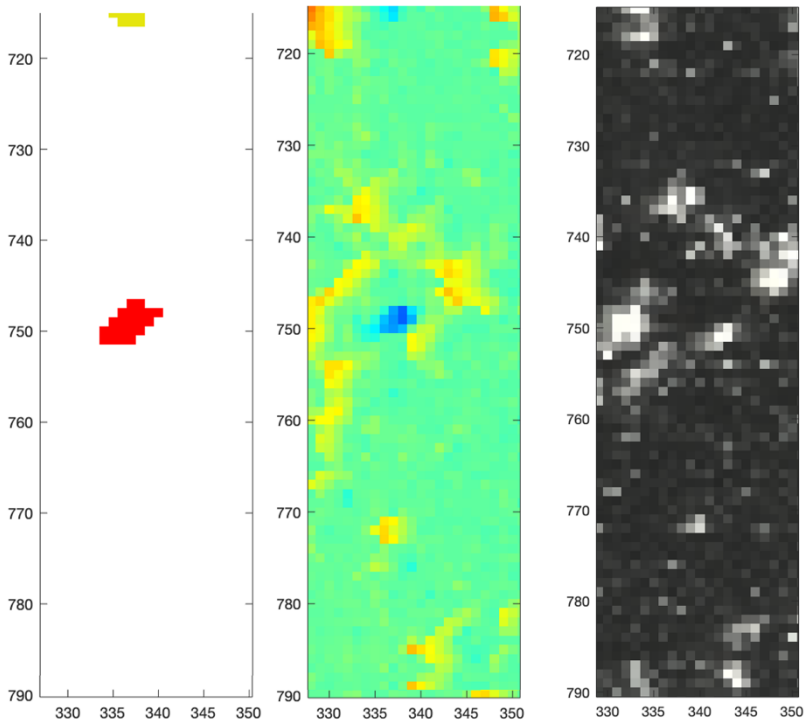

Figure 9a: Features from FY16DE05 Montage image with a depth of 63 microns. The montage pixel feature identification (left), height data (middle) and optical image (right). The features that are deeper are blue, higher are red and orange in the height image. Darker features in the optical image are indications of deeper features.

The feature flagged in the montage was found on the 20X LCM image from the x and y coordinates given in the montage image, which listed the feature as having a depth of 68 microns (Figure 9b).

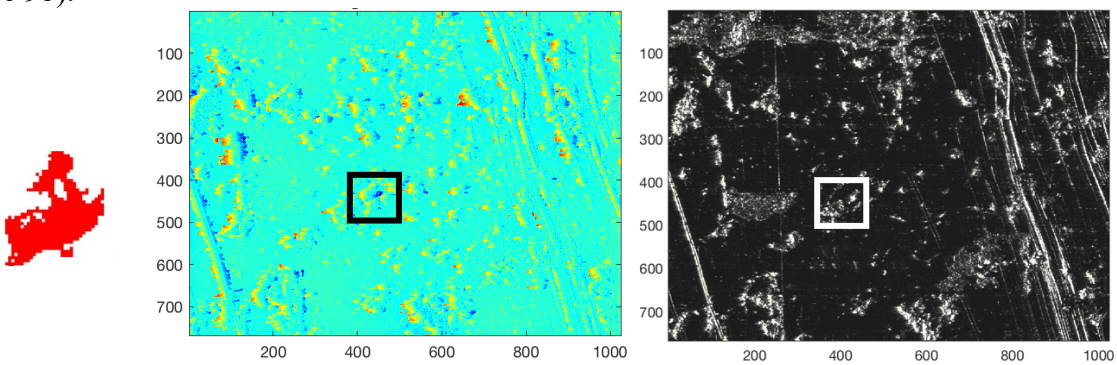

Figure 9b: Features from FY16DE05 individual 20X image with a depth of 68 microns. The individual 20X pixel feature identification zoomed in (left), height data where blue features are deep and red are high (middle) and optical image (right).

The distribution of the depths of the features for each container are shown in Figure 10, where the x axis is the depth (in microns) and the y axis is the number of features at the various depths. The pit features from the three containers range from 20 to 82 microns, where 20 microns was the minimum threshold set by the analyst. Container FY16 DE05 has the greatest number of pit features, but many of them are smaller features. The majority of the features for all three

containers have depths below 40 microns (black vertical line), as selected by the analyst for features of interest which equates to about 94% of the pit depths across all three containers.

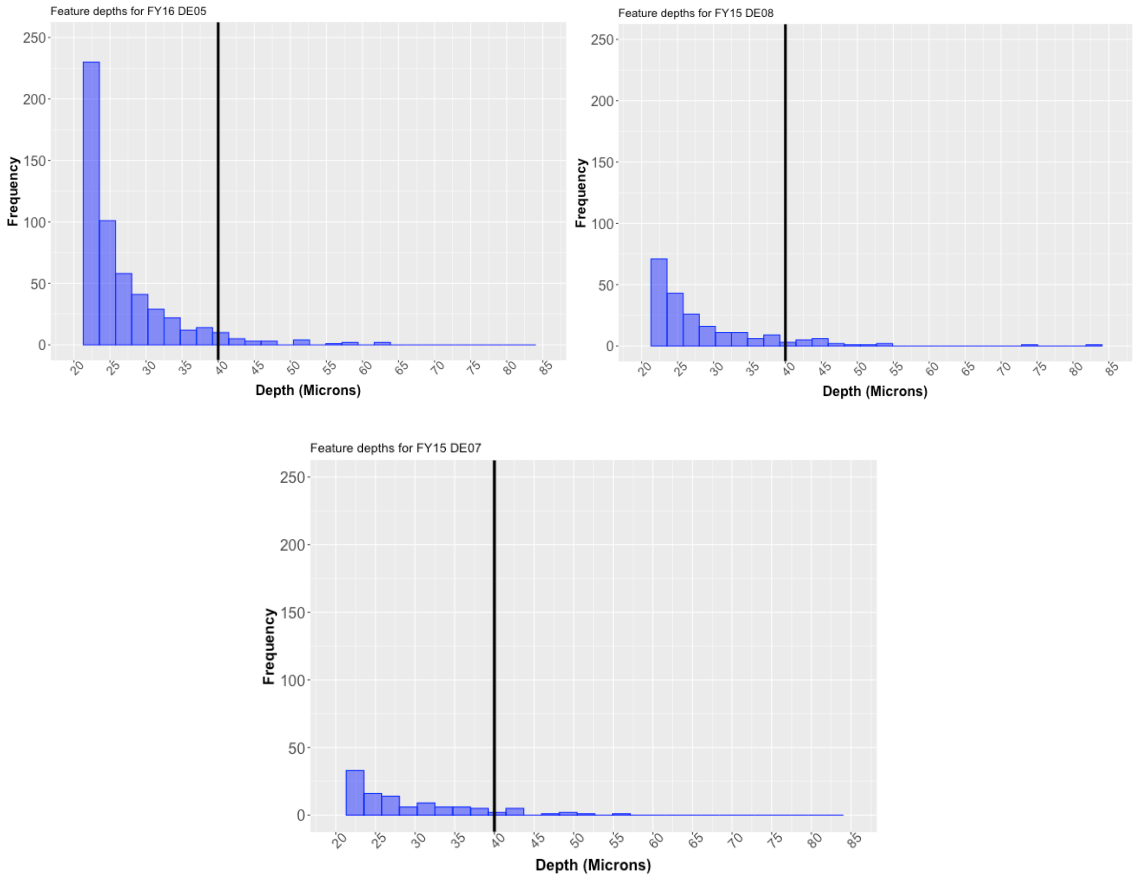

Figure 10: Histograms for the depth distributions for FY16DE05 (top left), FY15DE08 (top right), and FY15DE07 (bottom). The black line is the 40 micron mark, 94% of the features have depths below this value.

One of the other metrics of interest is volume. Volume is a direct measure of how much wall material was removed by corrosion (assuming the whole bottom of the feature is visible in LCM height imaging). The distribution of the volumes is shown in Figure 11 where the volume is in cubic microns. The majority of the features have volumes less than 250,000 cubic microns or 0.00025 cubic millimeters (black vertical line on figures), a cutoff that is equal to half an ideal hemispherical pit of approximately 100 microns in diameter (50 microns in depth). The largest feature in terms of volume was found to be in FY15 DE07 with a volume of 0.00054 cubic millimeters (540,000 cubic microns), considerably larger than the maximum volumes in the other two containers. If this were the volume from an idealized spherical pit, one would expect a depth of approximately 130 microns whereas the depth of this pit is 57 microns. FY15 DE07 has a higher frequency of feature volumes greater than 250,000 cubic microns and also has more large volume features compared to the other two containers.

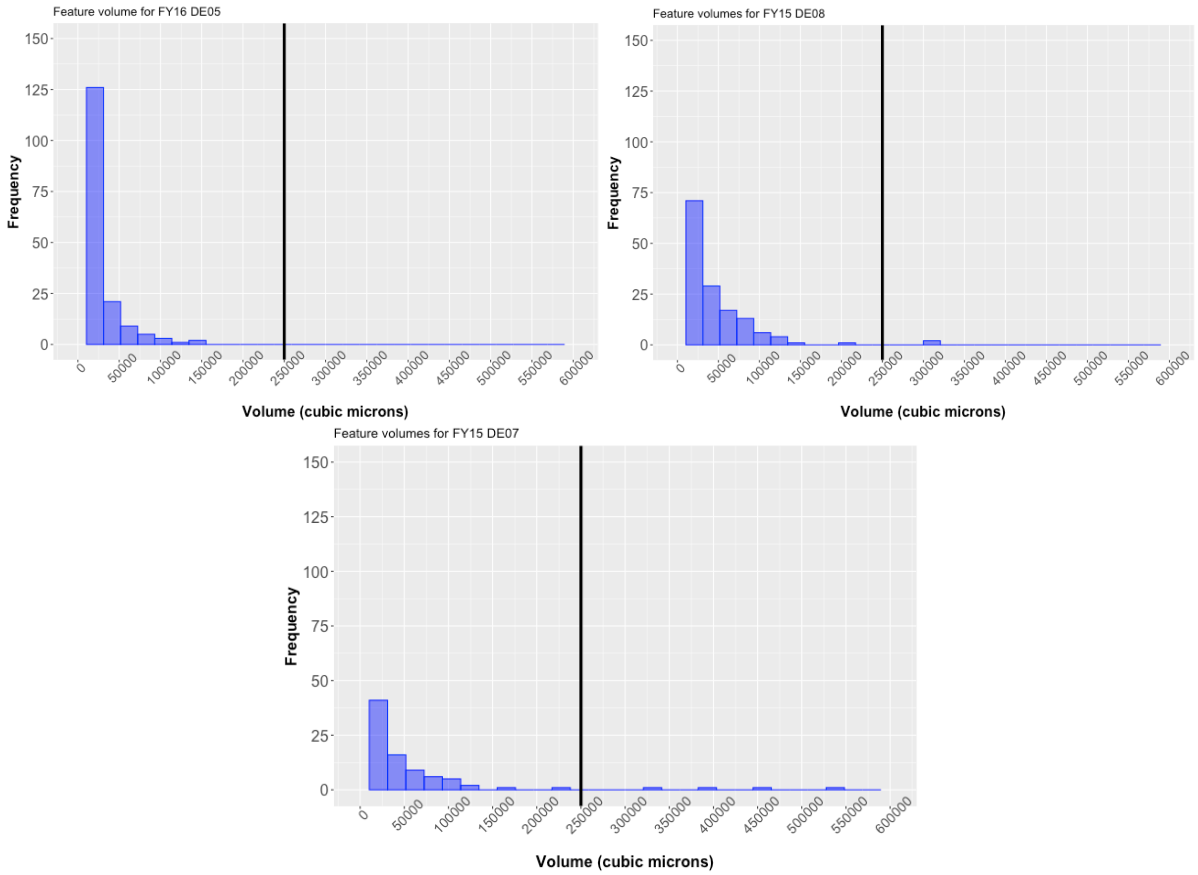

Figure 11: Histograms of the volumes for each of the three containers, FY16DE05 (top left), FY15DE08 (top right) and FY15DE07 (bottom). The black line shows that most of the containers are below 250,000 cubic microns.

The distributions of the equivalent diameters for the three containers are shown in Figure 12, where the equivalent diameter is in microns on the x axis and the frequency of the equivalent diameter is on the y axis. The equivalent diameters range from 5 to 164 microns, where most of the features have equivalent diameters that are less than 80 microns (black vertical line on the figures), as chosen by the analyst from doubling the 40 micron depth value in Figure 10. Diameters less than 80 microns accounts for approximately 92% of the diameters from all three contianers analyzed.

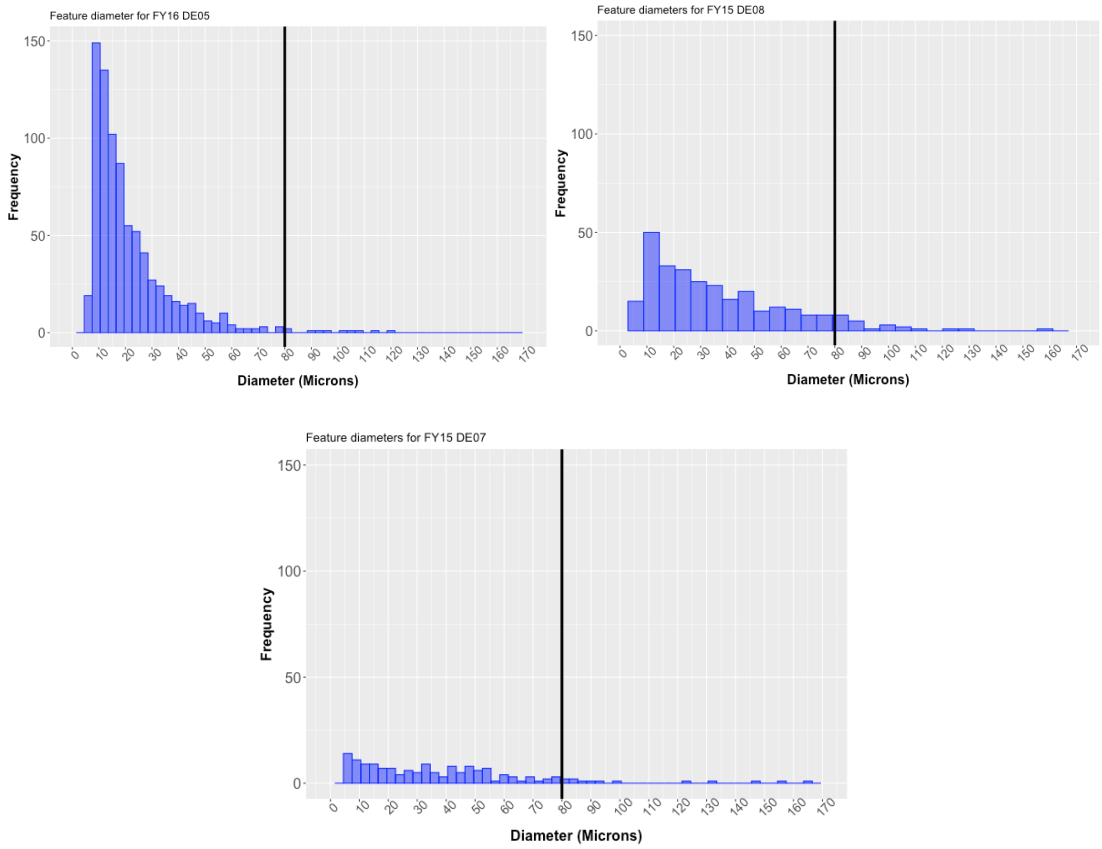

Figure 12: Histograms for equivalent diameter for all three containers, FY16DE05 (top left), FY15DE08 (top right) and FY15DE07 (bottom). The black line is 80 microns, most of the containers equivalent diameters are less than this value.

Figure 13 shows the relationship between depth and equivalent diameter for each of the three containers. Spherical shaped features have a depth approximately equal to ½ the diameter (the black line on the figures). Note that for all three containers many features are deeper than would be expected if they were approximately spherical (features above black line). Those features below the black line are not as deep as expected if spherical and may be conglomerated features.

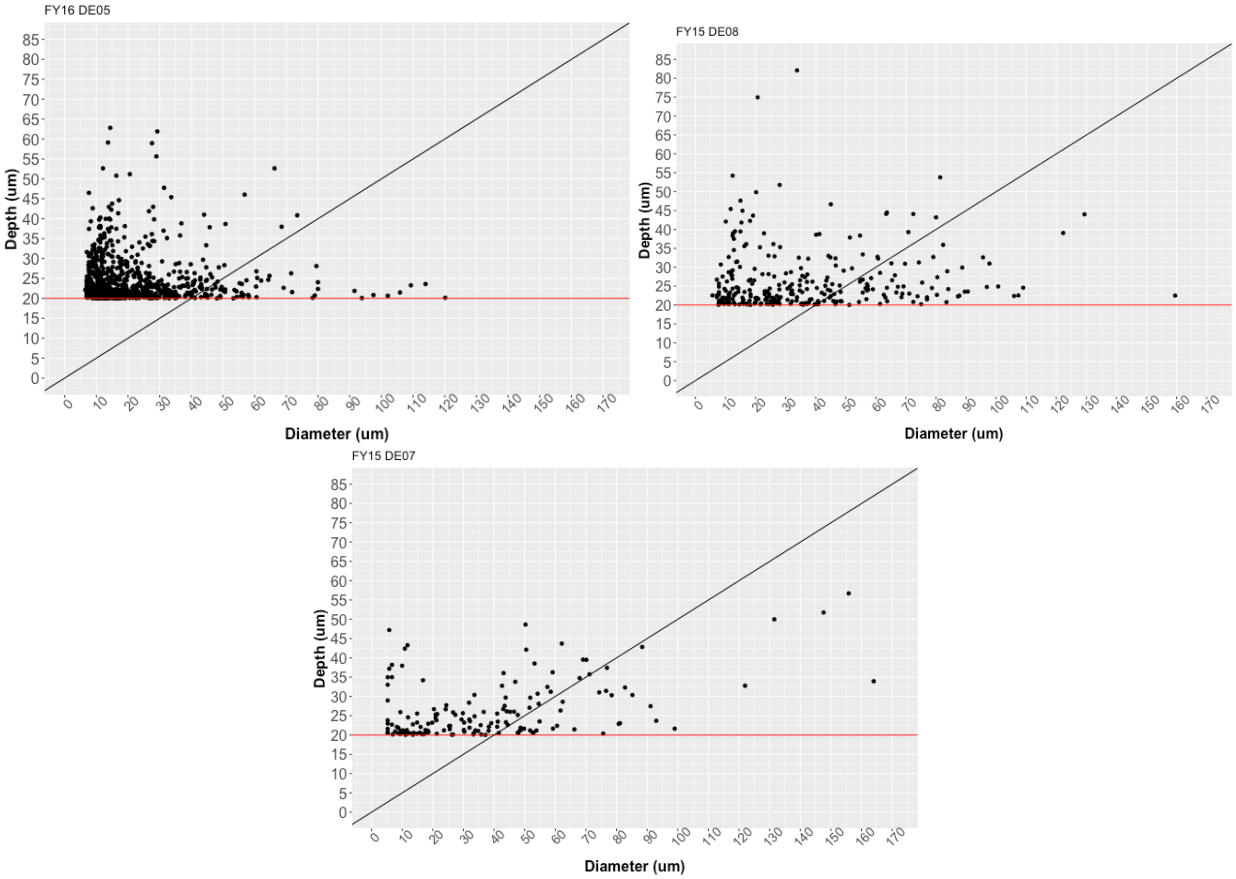

*Figure 13: Equivalent Diameter verses Depth scatterplots for FY16DE05 (top left), FY15DE08 (top right) and FY15DE07 (bottom center). The red line is the 20 micron threshold and the black line is the Depth = 1/2*Diameter line.*

4.3 DE Results and Time Extrapolation of Pit Depths Using the Pit Growth Model

A statistical framework was developed for determining and comparing predictions of corrosion pit depth growth based on multiple data sets collected under different experimental and environmental conditions (Kelly, et al 2014). Two of the data sets evaluated in the framework document are relevant for comparing to the pit depth results for the three ICCWRs. The first, the ARF-H data, are from an experimental small-scale container made of 304L stainless steel loaded with ten grams of impure radioactive oxide (ARF material) and 0.5 wt% water (Veirs, et al. 2004). The H stands for headspace region. The data consist of all suspected pits greater than 10 microns that could be observed in the headspace region based on Scanning Electron Microscope (SEM) imaging. Depths were not actually measured but were estimated based on the width of the pit. The pit depth was assumed to be half the width. The pits were evaluated after three months of exposure.

The second data set, the Zapp data, is from Phil Zapp's examination of pits from a 3013 surveillance container, FY09DE02 H004111 (Kelly, et al 2014). These data consist of suspected pit depths measured from the inner can lid of FY09DE02 that had been in storage for five years. The material in the container was radioactive oxide with chlorine and other impurities with a water content of 0.26 wt%. The inner container lid had the worst pitting corrosion seen to date in

a DE container. The Zapp data used a section or slice of the lid to examine pit depths. Depths were determined using scanning electron microscopy (SEM). The edge of the pit was focused on and then the pit bottom. The z movement was used as the pit depth. The slice was chosen randomly, since corrosion was fairly uniform around the circumference of the lid. The area of the slice was 2 cm^2. The entire area of the slice was examined by SEM to assess the pitting (Kelly and Mickalonis, 2021).

The pit growth model used in the statistical framework is $Depth = \beta t^b$. This power-law pit growth model is used in many applications and there is considerable physical and empirical justification for its use (Laycock et al. 1990, ASTM Standard G46 2005, Ricker 2005). The model does not depend on an assumption of spherical pits. Beta (β) is determined from the data. In the statistical framework the value of 0.5 is used for the parameter b. This value for b is widely used and there is also underlying physical and empirical evidence supporting its use as noted in the references. In addition, experiments by Juan Duque with teardrops support this value (Duque et al., 2012). It should be noted that the power-law pit growth model with b = 0.5 means that the slope of the pit gowth curve decreases over time.

Table 4 shows the results of the max pit depth from the model predictions compared to the actual maximum pit depth measurements for FY15DE08, DY16DE05, and FY15DE07.

Table 4. Pit growth model predictions compared to results from the three complete ICCWRS

	Time to Measurement	**Deepest pit depth measured (microns)**	**Predicted (red) or measured max depth (~12 years) (microns)**	**Model-based 95% Upper Quantile for max at 12 years (microns)**	**Expected Max Depth in 50 years (based on pit growth model)** (microns)	**Model-based 95% Upper Quantile for max at 50 year (microns)**
Zapp Data in Model (headspace)	5 years	23	40	90	80	180
ARF Data in Model (headspace)	3 months	25	200	380	395	700
FY15DE08 Zone 3	12 years	82	82	NA	167	NA
FY16DE05 Zone 3	12 years	63	63	NA	129	NA
FY15DE07 Zone 3	12 years	57	57	NA	116	NA

The complexity and uncertainties in the model-based results come from estimating max depth from small data sets versus knowing the max depth for DEs, as in the case of the three complete

ICCWRS. Therefore, it makes sense to compare the measured max values at 12 years to the model-based 95% upper quantiles for the predicted max at 12 years. The Zapp predicted value for the 95% quantile at 12 years is 90 microns and the observed max values at 12 years are 82, 63 and 57 microns for FY15DE08, FY16DE05 and FY15DE07, respectively. The ARF data were collected after only three months leading to the largest uncertainties and its 95% quantile at 12 years is 380 microns. Therefore, the observed pitting found on FY15DE08, FY16DE05 and FY15DE07 is consistent with model predictions based on the Zapp data and bounded by the ARF predictions. The model-based predicted max depth at 50 years based on the Zapp data is 180 microns and the predicted max depth for the ARF data is 700 microns. The estimated max depth values at 50 years using the observed β's in the power-law growth curve for FY15DE08, FY16DE05 and FY15DE07 are 167, 129, and 116, respectively. Again, consistent with the Zapp predictions and bounded by the ARF predictions.

5 Summary and discussion

This pitting analysis of the three containers with complete 20X LCM imaging was done using the automated software to analyze the montage images. The analysis showed that the montage results were consistent with the results of the individual 20X images. The analysis also showed that for the three complete ICCWR examination containers potential pit depths did not exceed 82 microns and the majority of potential pit depths were less than 40 microns.

The plots of depth verses equivalent diameter show that the majority of potential pits are not spherical. Most are deeper than would be expected if they were spherical, however, many have diameters that are greater than would be expected if spherical.

The histograms show considerable differences in numbers of pits, pit depths and volumes for the three containers. FY15DE07 had fewer potential pit features than the other two containers, yet it has more potential pits with large equivalent diameters and large volumes and is known to have the largest stress corrosion cracks observed on the ICCWR surface. These differences could be from differences in the composition or the concentrations of corrosive gases, or the time exposed to the gases. Longer exposure time may cause pits to grow deeper, volumes to become larger and more pits to form. But FY15DE07 has fewer pits than the other two containers. This suggests that differences in gas composition or concentration, more than time exposed, are responsible for the differences in the histograms, and that the conditions in FY15DE07 are more aggressive once pits are formed. It also indicates that the conditions in FY15E07, while aggressive once pits are formed, do not initiate pits as readily as the conditions in the other two containers.

The potential pit depths for the three containers were compared to model-based predictions. This comparison showed that the potential pit depth measurements were bounded by or consistent with the model-based predictions. This result further validates the model-based predictions and supports the assumption that through-wall pitting is not an issue for 3013 containers.

Acknowledgements
The authors would like to thank Dr. John Berg and Dr. Kirk Veirs for their thorough reviews of this report. Their questions, comments and suggestions greatly improved the report. In particular,

Dr. Veirs comments on the implications of the differences between the three containers as seen in the histograms greatly improved the Summary section.

This work has also benefited from information and guidance from Dr. Juan Duque. In addition to answering multiple questions, Dr. Duque has provided Keyence images that, along with Dr. Berg's Gwyddion images, were used for comparison to the automated software images.This report is based on several presentations to the LANL Corrosion Working Group (LANL CWG) chaired by Dr. Daniel Rios. The authors are grateful for the insightful comments and suggestions provided by the LANL CWG during and after the presentations.

None of this analysis could have been done without the imaging data and support of Dr. Michael Martínez-Rodríguez and his team at SRNL. Thank you for answering all of our questions and providing such excellent data.

References

1. ASTM Standard G46. (2005), "Standard Guide for Examination and Evaluation of Pitting Corrosion," *ASTM International*, West Conshohocken, PA, **DOI:** 10.1520/G0046-94R05, www.astm.org.
2. Berg, J. M., D. K. Veirs, E. J. Kelly, J. G. Duque, S. A. Joyce, J. E. Narlesky, J. M. Duffey, J. I. Mickalonis and K. A. Dunn. (2014). Test Plan for Assessing Potential for Stress Corrosion Cracking in the 3013 Inner Container Closure Weld Region (FY 2014). Los Alamos National Laboratory report LA-UR-14-20785, August, 2014.
3. DOE (Department of Energy). 2015. Integrated Surveillance and Monitoring Program for Materials Packaged to Meet DOE-STD-3013, *AMNMS-15-0014*, May 2015.
4. Duque, J.G., Rios, D., Patterson, B.M., Kuettner, L.A., Martinez-Rodriguez, M. (2020a). FY15-DE07 C1 and C2 Imaging Results. Los Alamos National Laboratory report LA-UR-20-30286, December, 2020.
5. Duque, J.G., Rios, D., Patterson, B.M., Kuettner, L.A., Hill, M.A., Bohn, K.R., Martinez, M.(2020b). Methods of measuring corrosion features on the surface of Inner containers and the extent of sub-surface 3013 Surveillance and Monitoring Annual Program Review. LA-UR-20-20930, January 2020.
6. Duque, J.G., Kaufeld, K.A., Kelly, E.J. (2018). Depth Analysis for Baseline Data and Implications for Future ICCWR Examinations, LA-UR-18-27490.
7. Kaufeld, K.A. Wendelberger, J.G., Kelly, E.J., Rodriguez-Martinez, M. (2021a) Montage pit assessment of FY15 DE08, LA-UR-21-21762.
8. Kaufeld, K.A. Wendelberger, J.G., Kelly, E.J., Rodriguez-Martinez, M. (2021b). Montage (stitched 20X images) Pit Assessment of FY16 DE05. LA-UR-21-21764,
9. Kaufeld, K.A. Wendelberger, J.G., Kelly, E.J., Rodriguez-Martinez, M. (2021c). Automated Pit Depth Analysis for Montage Images of ICCWR from Three DE Containers LA-UR-21-21611.
10. Kelly, E.J., Graves, T.L., Veirs, D.K., Duque, J.G. (2017). A Statistical Framework for Comparison of Predictions of Corrosion Pit Depth Growth Based on Multiple Data Sets Collected Under Different Experimental and Environmental Conditions, Los Alamos National Laboratory report LA-UR-14-28129, October 2017.

11. Kelly, E.J and Mickalonis, J.I. (2021). August 2012 Email from John Mickalonis to Elizabeth Kelly Answering Questions About the Zapp Data. LA-UR-21-30310.
12. Laycock, P.J., R. A. Cottis and P. A. Scarf. (1990), "Extrapolation of Extreme Pit Depths in Space and Time," *Journal of Electrochemical Society,* Vol. 137, No. 1. 64-69.
13. Martínez-Rodríguez, M.J., Laser Confocal Microscope for Analysis of 3013 Inner Container Closure Weld Region. SRNL-STI-2017-00589 Revision 0. October 2017.
14. Martínez-Rodríguez, M.J., Status of the Full Circumference Examination of the Inner Container Closure Weld Region for Selected 3013 DE Containers, (2018). SRNL-L4400-2018-00017 Revision 0. July 30, 2018.
15. Martínez-Rodríguez, M.J., FY19 Status of the Full Circumference Examination of the Inner Container Closure Weld Region for Selected 3013 DE Containers. SRNL-L5400-2019-00011 Revision 0. July 25 2019.
16. Ricker, R. E. (2010), "Analysis of Pipeline Steel Corrosion Data From NBS (NIST) Studies Conducted Between 1922-1940 and Relevance to Pipeline Management," *Journal of Research of the National Institute of Standards and Technology*, Volume 115, Number 5, 373-392.
17. Veirs, D. K., Padilla, D.D., Carillo, A., Martinez, M., Montya, A. (2004). Gas Generation and Corrosion in Salt-Containing Impure Plutonium Oxide Materials. Los Alamos National Laboratory report LA-UR-04-1788, March 2004.
18. Wendelberger, J.G., Kelly, E.J., Kaufeld, K.A., Berg, J. (2020) Pit and Crack Detection Summary Report FY 15 DE 07 Zone 3 TS20200813162639. Los Alamos National Laboratory report Los Alamos National Laboratory report LA-UR-20-26417, August 2020.